

doi: 10.12029/gc20170310

张玉,裴先治,李瑞保,刘成军,陈有忻,李佐臣,王兴,胡晨光,颜全治,彭思钟. 2017. 东昆仑东段阿拉思木辉长岩锆石U-Pb年代学、地球化学特征及洋盆闭合时限界定[J]. 中国地质, 44(3): 526–540.

Zhang Yu, Pei Xianzhi, Li Ruibao, Liu Chenjun, Chen Youxin, Li Zuochen, Wang Xin, Hu Chenguang, Yan Quanzhi, Peng Sizhong, Chen Guochao. 2017. Zircon U-Pb geochronology, geochemistry of the Alasimu gabbro in eastern section of East Kunlun Mountains and the closing time of Paleo-ocean basin[J]. Geology in China, 44(3): 526–540(in Chinese with English abstract).

东昆仑东段阿拉思木辉长岩锆石U-Pb年代学、地球化学特征及洋盆闭合时限界定

张玉^{1,2} 裴先治^{1,2} 李瑞保^{1,2} 刘成军^{1,2} 陈有忻^{1,2} 李佐臣^{1,2}
王兴^{1,2} 胡晨光^{1,2} 颜全治^{1,2} 彭思钟^{1,2}

(1.长安大学地球科学与资源学院,陕西西安710054;
2.长安大学西部矿产资源与地质工程教育部重点实验室,陕西西安710054)

提要:东昆仑东段广泛分布晚古生代的中酸性花岗岩,基性岩浆岩记录较少。本文选择位于东昆仑北弧岩浆带南缘的阿拉思木基性岩进行研究,为东昆仑东段晚古生代岩浆演化研究提供新的依据。通过LA-ICP-MS锆石U-Pb定年方法获得阿拉思木基性岩形成年龄为(241±1)Ma,为中三叠世岩浆活动的产物。岩石地球化学特征显示岩石具有低TiO₂(0.17%~0.37%,平均值0.25%)和较高的Mg[#]值(72.94~77.32,平均值为74.95)及Al₂O₃值(13.08~23.20%,平均值18.9%),富集大离子亲石元素(LILE: Sr、Rb、Ba),明显亏损高场强元素(HFSE: Nb、Ta、Zr、Hf)。Harker图解表明,MgO与Fe₂O₃、TiO₂、Ni、Co呈明显的正相关,暗示阿拉思木基性岩浆在形成过程中有一定程度的橄榄石、钛铁氧化物的分离结晶。阿拉思木辉长岩具有岛弧玄武岩的地球化学特征,并且其结晶年龄明显早于东昆仑碰撞及后碰撞构造岩浆时限。综合区域地质资料认为,阿拉思木辉长岩可能代表了东昆仑地区中三叠世洋壳俯冲的最晚期岩浆记录,进而确定东昆仑古特提斯洋俯冲结束碰撞开始的时间可能为中三叠世。

关 键 词:东昆仑造山带;辉长岩;岛弧;锆石U-Pb定年;中三叠世

中图分类号:P597.3;P595 **文献标识码:**A **文章编号:**1000-3657(2017)03-0526-15

Zircon U-Pb geochronology, geochemistry of the Alasimu gabbro in eastern section of East Kunlun Mountains and the closing time of Paleo-ocean basin

ZHANG Yu^{1,2}, PEI Xianzhi^{1,2}, LI Ruibao^{1,2}, LIU Chenjun^{1,2}, CHEN Youxin^{1,2}, LI Zuochen^{1,2},
WANG Xin^{1,2}, HU Chenguang^{1,2}, YAN Quanzhi^{1,2}, PENG Sizhong^{1,2}

收稿日期:2016-04-22;改回日期:2016-06-02

基金项目:国家自然科学基金项目(41472191、41502191、41172186、310827161006)、中央高校基本科研业务费专项资金项目(CHD2011TD020、2013G1271091、2013G1271092)和青海省国土资源厅-中国铝业公司公益性区域地质矿产调查基金项目(中铝基金200801)联合资助。

作者简介:张玉,男,1991年生,硕士生,构造地质学专业;E-mail:2211461032@qq.com。

通讯作者:裴先治,男,1963年生,教授,博士生导师,从事构造地质学和区域地质学研究;E-mail:peixzh@263.net。

(1. School of Earth Science and Resources, Chang'an University, Xi'an 710054, Shaanxi, China;
 2. Key Laboratory of Western China's Mineral Resources and Geological Engineering, Ministry of Education, Chang'an University, Xi'an 710054, Shaanxi, China)

Abstract: Late Paleozoic intermediate-acid granitoids are widely distributed in the East Section of East Kunlun, but the records of basic magmatism are very insufficient. Alasimu mafic rocks on the southern margin of the arc magmatic rock belt in northern East Kunlun Mountains was selected as the study objective so as to provide a new basis for the research on the Late Paleozoic magmatic evolution of the east section of East Kunlun Mountains. LA-ICP-MS zircon U-Pb analysis yielded the crystallization age of 241 ± 1 Ma, suggesting that Alasimu Mafic rocks were formed in the Middle Triassic. All the rock samples are characterized by relatively low TiO_2 (0.17%–0.37%, averagely 0.25%) and high $Mg^{\#}$ (72.94%–77.32%, averagely 74.95%) and high Al_2O_3 (13.08%–23.20%, averagely 18.9%), enrichment of large ion lithophile elements (LILE: Sr, Rb, Ba), apparent depletion of high field strength elements (HFSE, Nb, Ta, Zr and Hf). MgO shows some correlation with $Fe_{2}O_3^T$, TiO_2 , Ni and Co in the diagram of Harker, which reveals some degree of fractional crystallization of olivine and Ti-Fe oxide. Alasimu mafic rocks have similar chemical composition to island arc basalts, and they formed earlier than the collision and post-collision time of tectonic-magmatic activity. Combined with regional studies, the authors hold that Alasimu gabbro rocks ought to be the latest magmatism records in the East Kunlun region related to Middle Triassic Paleo Tethys oceanic crust subduction, which indicated that the tectonic transition from ocean subduction to collisional orogeny might have commenced in Middle Triassic.

Key words: East Kunlun orogenic belt; gabbro; island arc; zircon U-Pb geochronology; Middle Triassic

About the first author: ZHANG Yu, male, born in 1991, master candidate, majors in structural geology; E-mail: 12211461032@qq.com.

About the corresponding author: PEI Xianzhi, male, born in 1963, doctor, supervisor of doctor candidates, mainly engages in the study of structural geology and regional geology; E-mail: peixzh@263.net.

Found support: Supported by the National Science Foundation of China (No. 41472191, 41502191, 41172186); the Special Fund for Basic Scientific Research of Central Colleges, Chang'an University (Nos. CHD2011TD020, 2013G1271091, 2013G1271092); the Commonweal Geological Survey, the Aluminum Corporation of Chian and the Land-Resources Department of Qinghai Province (No. 200801).

1 引言

东昆仑造山带是中央造山系的重要组成部分(许志琴等, 2006; 杨经绥等, 2010), 同时也是青藏高原内部可与冈底斯带相媲美的另一条巨型岩浆岩带(莫宣学等, 2007)。显生宙以来, 该造山带主要经历了原特提斯洋和古特提斯洋两期洋陆构造演化过程。特别是古特提斯阶段岩浆活动剧烈, 构成了东昆仑弧岩浆岩带主体。东昆仑晚古生代洋盆打开时间为晚泥盆—早石炭世(莫宣学等, 2007), 洋壳的俯冲作用至少在260 Ma左右已经开始(杨经绥等, 2005; 马昌前等, 2015), 大量发育225 Ma左右的后碰撞花岗岩和少量的伸展型镁铁质岩石(陈国超等, 2013; 李佐臣等, 2013; 奥琮等, 2015; 熊富浩等, 2014; 陈国超, 2014), 暗示晚三叠世东昆仑地区已经进入碰撞后构造演化阶段。然而对于洋壳俯冲最终结束和碰撞开始的时间仍存在争

论。一些学者(莫宣学等, 2007; 刘成东等, 2004; 谌宏伟等, 2005; 李碧乐等, 2012)通过对东昆仑造山带花岗岩的研究, 认为在240 Ma左右进入到了洋壳俯冲作用的晚期。但 Huang et al., (2014)对东昆仑花岗质岩石研究认为, 260~240 Ma花岗质岩石为同碰撞环境下洋壳部分熔融的产物, 布青山—阿尼玛卿洋也已经闭合。Ding et al.(2014)对东昆仑早三叠世花岗质岩脉研究发现, 其具有A2型花岗岩特征, 此时东昆仑进入到了后碰撞阶段。

位于东昆北弧岩浆岩带南缘的阿拉思木辉长岩体, 形成于中三叠世中期, 具有弧岩浆岩特征, 其对于探讨东昆仑地区古特提斯洋演化具有重要地质意义。因此, 本文研究选取都兰县巴隆地区哈图沟的阿拉思木辉长岩体为研究对象, 开展详细野外地质、岩石学、锆石U-Pb年代学和岩石地球化学研究, 综合分析岩石成因与构造环境, 为确定东昆仑晚古生代—早中生代洋壳俯冲与碰撞造山的转换

时限提供证据。

2 区域地质背景与岩体地质特征

东昆仑造山带位于青藏高原东北部,中国大陆中央造山系西段,南邻巴颜喀拉造山带,北邻柴木地块,其西被阿尔金大型走滑断裂所截并与西昆仑造山带相隔,东至秦(秦岭造山带)—昆(昆仑造山带)岔口,东西延伸约1500 km,处于古亚洲洋构造域和特提斯—喜马拉雅构造域的结合部位(殷鸿福等,2003)。东昆仑造山带由北向南可划分为东昆北构造带、东昆中蛇绿混杂岩带、东昆南构造带和阿尼玛卿—布青山构造混杂岩带(图1)。研究区位于东昆北构造带,主要以大面积分布前寒武纪变

质基底和加里东—印支期花岗岩类为特征。白沙河岩组(Pt_1b)和小庙岩组(Pt_2x)在带内广泛分布,白沙河岩组主要由大理岩、片麻岩、混合岩和斜长角闪岩组成,其原岩为碳酸盐岩、海相砂泥质碎屑岩和中基性火山岩等,形成年龄可约束在2.0~1.9 Ga(王国灿等,2007);小庙岩组主要由石英岩、大理岩、片麻岩和片岩组成,其原岩为浅海相碎屑岩和碳酸盐岩等,形成时代可约束在1.7~1.6 Ga(陈有忻等,2011);此外还有少量泥盆系、石炭系海相碳酸盐岩和碎屑岩沉积建造。东昆中缝合带或蛇绿混杂岩带沿着东昆中断裂带分布,展布于东昆仑山主脊位置,西起博卡雷克塔格,东至大干沟、清水泉、青根河和鄂拉山,并被北西向延伸的鄂拉山断裂截

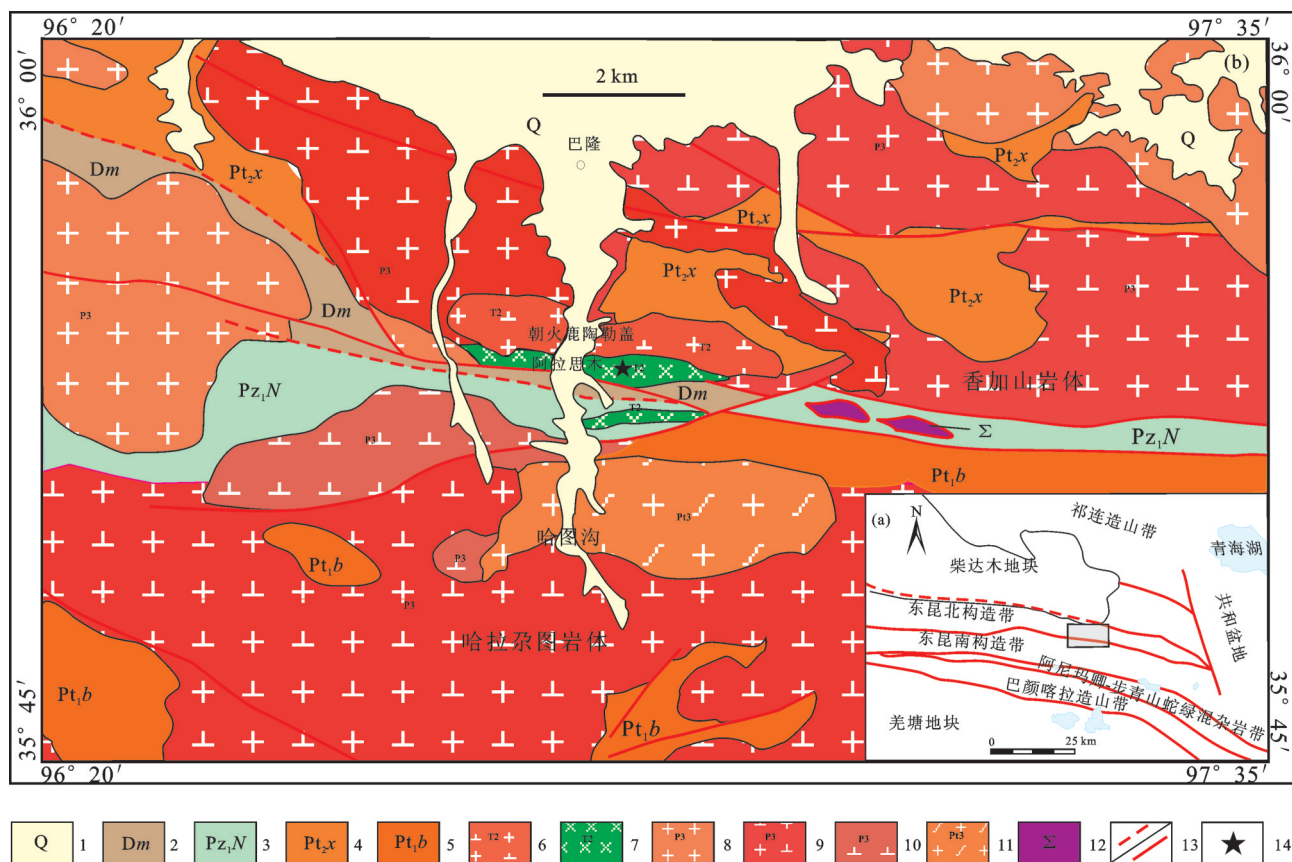


图1东昆仑东段巴隆地区地质简图

1—第四系;2—泥盆系牦牛山组;3—下古生界纳赤台岩群;4—中元古界小庙岩组;5—古元古界白沙河岩组;6—中三叠世花岗闪长岩;7—中三叠世辉长岩;8—晚二叠世花岗岩;9—晚二叠世花岗闪长岩;10—晚二叠世闪长岩;11—新元古代花岗质片麻岩;12—蛇绿岩;13—断层;14—采样位置

Fig. 1 Geological sketch map of Balong in the east part of Eastern Kunlun Mountains

1—Quaternary;2—Devonian Maoniushan Formation;3—Lower Paleozoic Nachitai Group;4—Mesoproterozoic Xiaomiao Formation;5—Palaeoproterozoic Baishahe Formation;6—Middle Triassic granodiorite;7—Middle Triassic gabbro;8—Late Permian granite;9—Late Permian granodiorite;10—Late Permian diorite;11—Neoproterozoic granitic gneiss;12—Ophiolite;13—Fault;14—Sampling location

断。带内分布有巴隆、清泉沟—阿此特、乌妥、清水泉、塔妥及曲什昂、可可沙—可可科特等蛇绿混杂岩块,呈近东西向延伸,带内多个蛇绿岩岩块及岛弧型岩浆岩分别呈岩块状产于古元古代、早古生代变质地层中,并卷入有晚古生代—早中生代沉积岩系(魏博,2015)。东昆南构造带以大量发育前寒武纪基底变质岩系(白沙河岩组、小庙岩组及万宝沟岩群)为特征。带内南缘出露下古生界纳赤台岩群、石炭系海相碳酸盐岩—碎屑岩沉积组合夹少量火山岩系、上二叠统格曲组粗碎屑岩和碳酸盐岩组合以及三叠系一下侏罗统海相、海陆交互相及陆相沉积地层。带内前寒武纪变质基底中发育加里东期弧型石英闪长岩,带中部发育大面积晚海西期—印支期花岗岩类。布青山—阿尼玛卿构造混杂岩带中基质主要由二叠系马尔争组复理石组成,其间至少混杂有早古生代和晚古生代两期蛇绿岩岩块以及包括中元古界苦海岩群(Pt₂K)变质基底岩块、晚奥陶世—早志留世岛弧型花岗岩与中酸性火山岩岩块、石炭纪海山玄武岩/灰岩岩块等复杂的混

杂岩块系统。Bian et al.(2004)研究提出布青山地区存在两套时代不同的蛇绿岩。刘战庆等(2011)测定布青山地区得力斯坦和哈尔郭勒两处蛇绿岩中辉长岩的锆石U-Pb年龄为(516±6) Ma和(333±3) Ma,再次表明该区可能存在不同时代的蛇绿岩。

本文报道的阿拉思木辉长岩体位于东昆北构造带南缘,南侧与东昆中蛇绿混杂岩带毗邻,近东西向展布(图1)。岩体主体侵入于泥盆系牦牛山组(D_{1m}),南侧与东昆中缝合带中的纳赤台岩群呈断层接触,北侧被朝火鹿陶勒盖花岗闪长岩体侵入(陈功等,2016)(图1)。阿拉思木辉长岩呈灰黑—深灰色,细粒辉长结构、块状构造,岩体未发生变形。主要矿物组成为斜长石(60%~65%)、辉石(15%~20%)、角闪石(5%~10%),斜长石呈灰白色自形—半自形板柱状,可见聚片双晶,具一定钠黝帘石化;辉石呈暗绿色自形粒柱状、短柱状结构,镜下可见两组近垂直节理,还见透闪石、黑云母化;角闪石呈半自形柱状,多色性明显,部分蚀变为黑云母、绢云母;其他矿物约占5%(图2)。

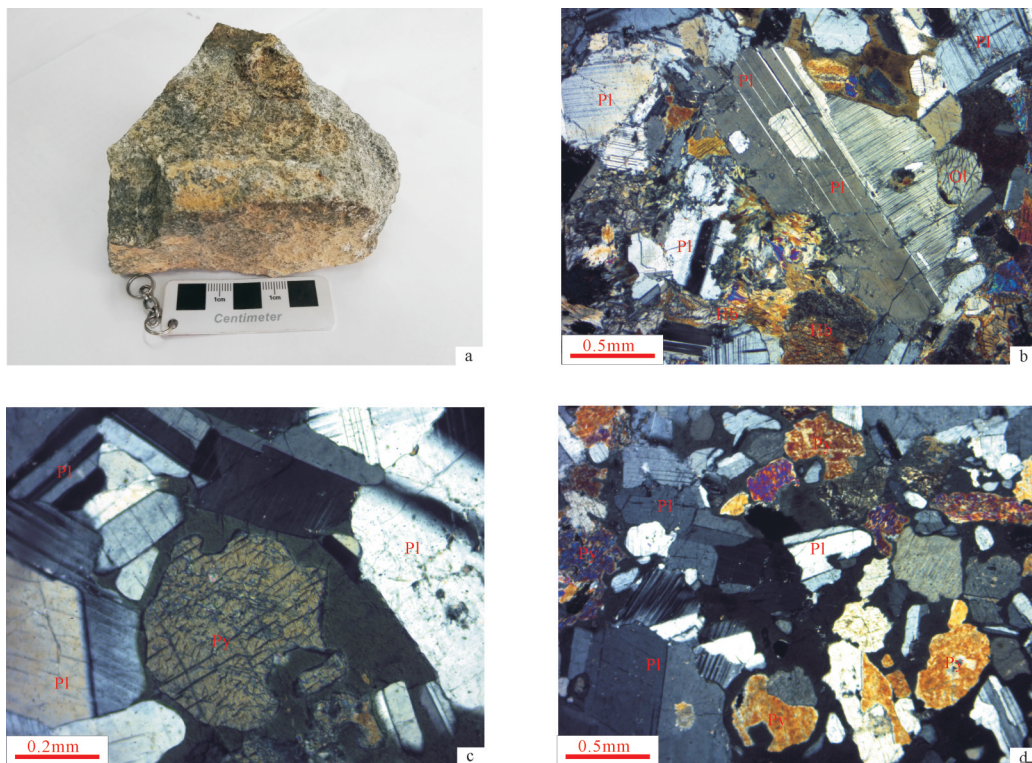


图2 阿拉思木辉长岩手标本及镜下显微照片

a—辉长岩手标本,b、c、d—均为显微镜下照片:Pl—斜长石;Ol—橄榄石;Hb—角闪石;Py—辉石

Fig. 2 Macrophotographs and microphotographs of samples

a—Petrographical photos of the sample;b, c, d—Microphotographs of samples:Pl—Plagioclase,Hb—Hornblende,Py—Pyroxene

3 样品采集与测试方法

用于分析测试的锆石U-Pb年代学样品以及岩石地球化学样品均采自阿拉思木辉长岩体的新鲜露头,采样位置可见图1,测年采样点地理坐标:N:35°53'58.5"E;97°24'45.6"。样品岩性为灰黑—深灰色细粒辉长岩。

用于测年的锆石样品按常规重力和磁选方法分选,而后在双目镜下挑选晶形完好的无色透明锆石颗粒制作样靶,用环氧树脂固定,固定后抛光使锆石表面暴露,用于阴极发光(CL)研究和LA-ICP-MS锆石U-Pb同位素组成分析。阴极发光图像在北京锆年领航科技有限公司的扫描电镜加载阴极发光仪上完成。锆石U-Pb同位素组成分析在天津地质矿产研究所同位素年龄实验室的激光剥蚀电感耦合等离子质谱仪(LA-ICP-MS)上完成。分析仪器为配备有193 nmA Rf-excimer激光器的Geo-Las200M型(Microlas Gottingen Germany)激光剥蚀系统和Elan6100DRC型四级杆质谱仪。分析采用激光剥蚀孔径30 μm,剥蚀深度20~40 μm,激光脉冲为10Hz,能量为(32~36)mJ。测试中用人工合成的硅酸盐玻璃标准参考物质NIST610进行仪器最佳化。锆石年龄计算采用国际标准锆石91500作为外标校正,每测定5个分析点后插入一次标样测定,以确保标样和样品的仪器条件完全一致。在所测锆石样品分析前后各测一次NIST610,同时以²⁹Si作为内标测定锆石的U、Th、Pb含量。用锆石91500进行外标校正同位素组成。LA-ICP-MS分析的详细方法和流程见描述(李怀坤等,2009)。样品的同位素比值和元素含量数据处理采用GLITER(ver4.0, Macquarie University)程序,并采用Anderson软件对测试数据进行普通铅校正,年龄计算及谐和图绘制采用ISOPILOT(2.49版)软件完成。所有数据点年龄值的误差均为 1σ ,采用²⁰⁶Pb/²³⁸U年龄,其加权平均值具95%的置信度(Ludwig et al., 2001; Anderson et al., 2002)。

全岩主量元素测试采用XRF法,测试在长安大学西部矿产资源与地质工程教育部重点实验室完成,测定流程包括烧失量的计算和玻璃融熔制样两大步骤:①计算烧失量:将坩埚在烘箱内150°C干燥3 h后,称其重量W₁,加入约1 g样品,称样品重量

W₂;然后放入900°C的马弗炉中8 h,降温后放入干燥器静置20 min,随后称重得W₃。通过公式(LOI)=(W₁+W₂-W₃)/W₂计算出样品的烧失量(LOI);②玻璃融熔法制样:主量元素测定时首先称取样品0.50 g,以无水四硼酸锂和硝酸铵为氧化剂,倒入铂金坩埚中,再加入适量溴化锂,在1200°C左右振荡熔融制成玻璃薄片,使用X射线荧光光谱仪测定。全岩稀土和微量元素分析长安大学西部矿产资源与地质工程教育部重点实验室完成,采用Thermo-X7电感耦合等离子体质谱仪,分析精度和准确度优于10%。将200目以下样品(500 mg)置于PTFE坩埚,加入添加剂(1.0 mL高纯HF和1.5 mL高纯HNO₃),按照标准测试程序,反复添加、加热、冷却后,最后在离心管中稀释到50 mL;将所得溶液在电感耦合等离子体质谱仪(ICP-MS)上完成测定。

4 测试结果

4.1 锆石U-Pb定年

辉长岩样品所选锆石多为浅黄色—无色,透明或半透明,宽板状晶形,长50~150 μm不等,长宽比3:1。锆石内部较纯净,基本无裂纹和包裹体。锆石CL图像显示具有明显的岩浆条带构造,且其Th/U值均大于0.1,显示为岩浆锆石(图3)。

对阿拉思木辉长岩样品中的锆石进行同位素年龄测定,测定结果见表1。共测试21个点,其中最小值为235.0 Ma,最大值为244.9 Ma,加权平均年龄为(241.1±1.2)Ma(MSWD=3.4)(图4),该年龄代表阿拉思木辉长岩的结晶年龄。

4.2 岩石主量元素地球化学特征

本次研究共选取6件样品进行测试分析,分析结果见表2。阿拉思木辉长岩样品烧失量小,均不超过2%。岩体的SiO₂含量低,变化范围较小,为46.08%~48.92%,平均值为46.94%;Na₂O为0.43~0.78%,平均值0.67%;K₂O为0.10%~0.56%,平均值0.24%;全碱含量较低(0.63%~1.33%),平均值为0.91%,Na₂O/K₂O平均值3.57;TiO₂含量较低(0.17%~0.37%),平均值为0.25%,明显低于洋脊拉斑玄武岩(1.5%)和洋岛拉斑玄武岩(2.63%),也不同于板内玄武岩(2.23%)及板内碱性玄武岩(2.9%),相对接近岛弧型玄武岩(0.98%)(Pearce et al., 1982);MgO含量较高,变化较大,6.12%~11.72%;Al₂O₃含

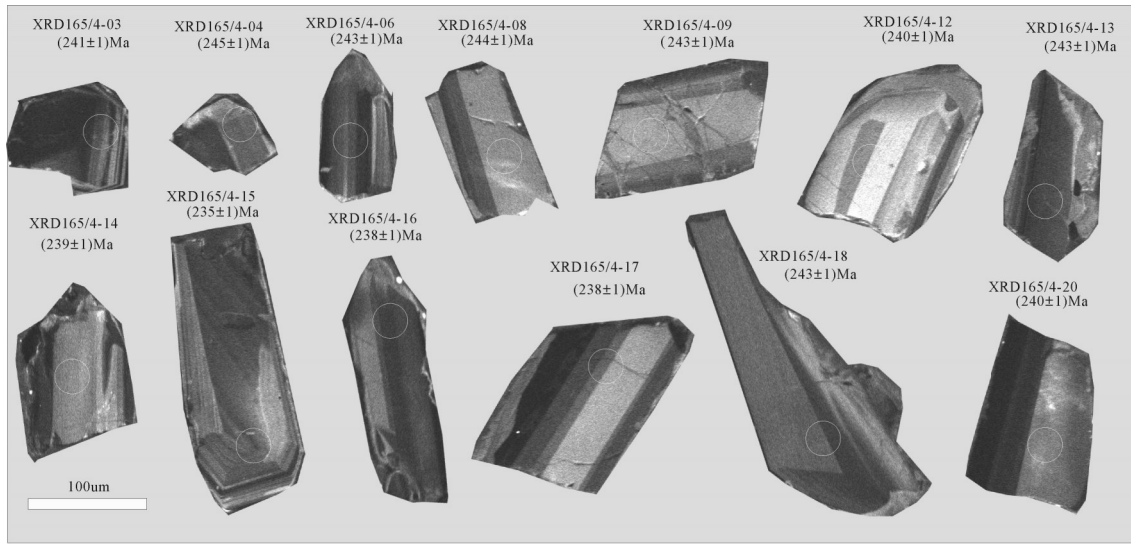


图3 阿拉思木辉长岩典型锆石CL图像与表面年龄

Fig.3 Representative cathodoluminescence images and apparent age of zircons from Alasimu gabbro

量较高,为13.08%~23.20%,平均为18.9%,类似高铝玄武岩;Mg[#]较高,变化于72.94~77.32,平均为74.95,与原生岩浆相近(Mg[#]=68~75)(Wilson, 1989)。考虑到Na和K活动元素易受蚀变作用的影响,使用Nb/Y-Zr/TiO₂×0.0001岩石分类图进行分类,样品均落入玄武岩区域。由SiO₂-(Na₂O+K₂O)图解与SiO₂-FeO^T/MgO图解综合判断样品属于拉斑玄武岩系列向钙碱性玄武岩系列过渡类型(图5)。在以MgO为横坐标的哈克图解中,Fe₂O₃^T、Ti、Ni、Co与MgO呈明显的正相关关系(图6)。

4.3 岩石微量和稀土元素地球化学特征

阿拉思木辉长岩的ΣREE含量较低,为9.39~17.32×10⁻⁶,平均值为12.96×10⁻⁶,LREE/HREE为2.83~4.67,在球粒陨石标准化配分图中为弱右倾型,轻重稀土具有一定分异,富集轻稀土元素,亏损重稀土元素(图7a)。 δ Eu为0.65~0.87,具Eu负异常;在微量元素原始地幔标准化图中(图7b),大离子亲石元素(LILE:Sr、Rb、Ba等)富集,高场强元素(HFSE:Nb、Ta、Zr、Hf等)亏损,尤其Nb、Ta亏损明显,且其原始地幔标准化值均低于1,显示阿拉思木辉长岩为与俯冲相关的岛弧环境的产物。岩石的Nb含量为0.45×10⁻⁶~5.8×10⁻⁶、Ta含量为0.03×10⁻⁶~0.50×10⁻⁶,Nb/Ta比值为11.32~24.29,平均为19。Cr含量变化范围较大,介于12.07×10⁻⁶~411.54×10⁻⁶,平均为109.07×10⁻⁶;Ni含量较高,介于101.56×10⁻⁶

294.99×10⁻⁶,平均为240.31×10⁻⁶。

5 讨论

5.1 岩石成因

在Harker图解中,MgO与Fe₂O₃^T、TiO₂、Ni、Co呈明显的正相关,暗示阿拉思木岩体在形成过程中有一定程度的橄榄石、钛铁氧化物的分离结晶作用(Graham et al., 1995; Morra et al., 1997; Naumann et al., 1999);另一方面阿拉思木辉长岩的Mg[#]、Cr和Ni含量较高且变化较小,Mg[#]值为72.95~77.32,平均值为74.95,MgO为7.52%~11.72%,平均值为9.09%,略低于原生岩浆(Mg[#]=68~75,MgO=10.7%~13.8%),Cr、Co、Ni均低于原生岩浆(Tatsumi et al., 1981),也暗示阿拉思木镁铁质岩石形成过程中发生了岩浆结晶分异作用。此外,岩石Al₂O₃含量较高,13.08%~23.02%,平均值为18.92%(大于17%),且岩石属于由拉斑向钙碱性过渡系列,并具有低钾、贫碱的特征,均与高铝玄武岩类似(邓晋福等,2004)。实验岩石学表明,经含0.1%H₂O的pyrolite(地幔岩)在深度15~35 km、压力p=0.5~1GPa的环境下,部分熔融程度为2%~5%时一般形成高铝玄武岩浆。与高压下(p≥1.6 GPa)形成的高Al₂O₃的TTG具有强分馏稀土分布样式、重稀土亏损不同,该高铝玄武岩具有弱轻稀土富集、重稀土平坦特点,它可能是在较低压力条件(p=0.8 GPA)、但熔融程度

表1 阿拉思木辉长岩(XRD165/4)中锆石LA-ICP-MS U-Pb同位素年龄分析数据
Table 1 U-Pb isotopic composition of zircons in Alasimu gabbro (XRD165/4) measured by using LA-ICP-MS technique

Zircon ID	U (ppm)	Pb (ppm)	U/Pb (ppm)	年龄 (Ma)	误差 (Ma)
Z1	12.5	15.8	0.78	165.4	±1.5
Z2	13.2	16.5	0.79	165.4	±1.5
Z3	14.8	18.5	0.79	165.4	±1.5
Z4	15.5	19.2	0.79	165.4	±1.5
Z5	16.2	20.0	0.79	165.4	±1.5
Z6	17.0	21.0	0.79	165.4	±1.5
Z7	17.8	21.8	0.79	165.4	±1.5
Z8	18.5	22.5	0.79	165.4	±1.5
Z9	19.2	23.2	0.79	165.4	±1.5
Z10	20.0	24.0	0.79	165.4	±1.5
Z11	20.8	24.8	0.79	165.4	±1.5
Z12	21.5	25.5	0.79	165.4	±1.5
Z13	22.2	26.2	0.79	165.4	±1.5
Z14	23.0	27.0	0.79	165.4	±1.5
Z15	23.8	27.8	0.79	165.4	±1.5
Z16	24.5	28.5	0.79	165.4	±1.5
Z17	25.2	29.2	0.79	165.4	±1.5
Z18	26.0	30.0	0.79	165.4	±1.5
Z19	26.8	30.8	0.79	165.4	±1.5
Z20	27.5	31.5	0.79	165.4	±1.5
Z21	28.2	32.2	0.79	165.4	±1.5
Z22	29.0	33.0	0.79	165.4	±1.5
Z23	29.8	33.8	0.79	165.4	±1.5
Z24	30.5	34.5	0.79	165.4	±1.5
Z25	31.2	35.2	0.79	165.4	±1.5
Z26	32.0	36.0	0.79	165.4	±1.5
Z27	32.8	36.8	0.79	165.4	±1.5
Z28	33.5	37.5	0.79	165.4	±1.5
Z29	34.2	38.2	0.79	165.4	±1.5
Z30	35.0	39.0	0.79	165.4	±1.5
Z31	35.8	39.8	0.79	165.4	±1.5
Z32	36.5	40.5	0.79	165.4	±1.5
Z33	37.2	41.2	0.79	165.4	±1.5
Z34	38.0	42.0	0.79	165.4	±1.5
Z35	38.8	42.8	0.79	165.4	±1.5
Z36	39.5	43.5	0.79	165.4	±1.5
Z37	40.2	44.2	0.79	165.4	±1.5
Z38	41.0	45.0	0.79	165.4	±1.5
Z39	41.8	45.8	0.79	165.4	±1.5
Z40	42.5	46.5	0.79	165.4	±1.5
Z41	43.2	47.2	0.79	165.4	±1.5
Z42	44.0	48.0	0.79	165.4	±1.5
Z43	44.8	48.8	0.79	165.4	±1.5
Z44	45.5	49.5	0.79	165.4	±1.5
Z45	46.2	50.2	0.79	165.4	±1.5
Z46	47.0	51.0	0.79	165.4	±1.5
Z47	47.8	51.8	0.79	165.4	±1.5
Z48	48.5	52.5	0.79	165.4	±1.5
Z49	49.2	53.2	0.79	165.4	±1.5
Z50	50.0	54.0	0.79	165.4	±1.5
Z51	50.8	54.8	0.79	165.4	±1.5
Z52	51.5	55.5	0.79	165.4	±1.5
Z53	52.2	56.2	0.79	165.4	±1.5
Z54	53.0	57.0	0.79	165.4	±1.5
Z55	53.8	57.8	0.79	165.4	±1.5
Z56	54.5	58.5	0.79	165.4	±1.5
Z57	55.2	59.2	0.79	165.4	±1.5
Z58	56.0	60.0	0.79	165.4	±1.5
Z59	56.8	60.8	0.79	165.4	±1.5
Z60	57.5	61.5	0.79	165.4	±1.5
Z61	58.2	62.2	0.79	165.4	±1.5
Z62	59.0	63.0	0.79	165.4	±1.5
Z63	59.8	63.8	0.79	165.4	±1.5
Z64	60.5	64.5	0.79	165.4	±1.5
Z65	61.2	65.2	0.79	165.4	±1.5
Z66	62.0	66.0	0.79	165.4	±1.5
Z67	62.8	66.8	0.79	165.4	±1.5
Z68	63.5	67.5	0.79	165.4	±1.5
Z69	64.2	68.2	0.79	165.4	±1.5
Z70	65.0	69.0	0.79	165.4	±1.5
Z71	65.8	69.8	0.79	165.4	±1.5
Z72	66.5	70.5	0.79	165.4	±1.5
Z73	67.2	71.2	0.79	165.4	±1.5
Z74	68.0	72.0	0.79	165.4	±1.5
Z75	68.8	72.8	0.79	165.4	±1.5
Z76	69.5	73.5	0.79	165.4	±1.5
Z77	70.2	74.2	0.79	165.4	±1.5
Z78	71.0	75.0	0.79	165.4	±1.5
Z79	71.8	75.8	0.79	165.4	±1.5
Z80	72.5	76.5	0.79	165.4	±1.5
Z81	73.2	77.2	0.79	165.4	±1.5
Z82	74.0	78.0	0.79	165.4	±1.5
Z83	74.8	78.8	0.79	165.4	±1.5
Z84	75.5	79.5	0.79	165.4	±1.5
Z85	76.2	80.2	0.79	165.4	±1.5
Z86	77.0	81.0	0.79	165.4	±1.5
Z87	77.8	81.8	0.79	165.4	±1.5
Z88	78.5	82.5	0.79	165.4	±1.5
Z89	79.2	83.2	0.79	165.4	±1.5
Z90	80.0	84.0	0.79	165.4	±1.5
Z91	80.8	84.8	0.79	165.4	±1.5
Z92	81.5	85.5	0.79	165.4	±1.5
Z93	82.2	86.2	0.79	165.4	±1.5
Z94	83.0	87.0	0.79	165.4	±1.5
Z95	83.8	87.8	0.79	165.4	±1.5
Z96	84.5	88.5	0.79	165.4	±1.5
Z97	85.2	89.2	0.79	165.4	±1.5
Z98	86.0	90.0	0.79	165.4	±1.5
Z99	86.8	90.8	0.79	165.4	±1.5
Z100	87.5	91.5	0.79	165.4	±1.5
Z101	88.2	92.2	0.79	165.4	±1.5
Z102	89.0	93.0	0.79	165.4	±1.5
Z103	89.8	93.8	0.79	165.4	±1.5
Z104	90.5	94.5	0.79	165.4	±1.5
Z105	91.2	95.2	0.79	165.4	±1.5
Z106	92.0	96.0	0.79	165.4	±1.5
Z107	92.8	96.8	0.79	165.4	±1.5
Z108	93.5	97.5	0.79	165.4	±1.5
Z109	94.2	98.2	0.79	165.4	±1.5
Z110	95.0	99.0	0.79	165.4	±1.5
Z111	95.8	99.8	0.79	165.4	±1.5
Z112	96.5	100.5	0.79	165.4	±1.5
Z113	97.2	101.2	0.79	165.4	±1.5
Z114	98.0	102.0	0.79	165.4	±1.5
Z115	98.8	102.8	0.79	165.4	±1.5
Z116	99.5	103.5	0.79	165.4	±1.5
Z117	100.2	104.2	0.79	165.4	±1.5
Z118	101.0	105.0	0.79	165.4	±1.5
Z119	101.8	105.8	0.79	165.4	±1.5
Z120	102.5	106.5	0.79	165.4	±1.5
Z121	103.2	107.2	0.79	165.4	±1.5
Z122	104.0	108.0	0.79	165.4	±1.5
Z123	104.8	108.8	0.79	165.4	±1.5
Z124	105.5	109.5	0.79	165.4	±1.5
Z125	106.2	110.2	0.79	165.4	±1.5
Z126	107.0	111.0	0.79	165.4	±1.5
Z127	107.8	111.8	0.79	165.4	±1.5
Z128	108.5	112.5	0.79	165.4	±1.5
Z129	109.2	113.2	0.79	165.4	±1.5
Z130	110.0	114.0	0.79	165.4	±1.5
Z131	110.8	114.8	0.79	165.4	±1.5
Z132	111.5	115.5	0.79	165.4	±1.5
Z133	112.2	116.2	0.79	165.4	±1.5
Z134	113.0	117.0	0.79	165.4	±1.5
Z135	113.8	117.8	0.79	165.4	±1.5
Z136	114.5	118.5	0.79	165.4	±1.5
Z137	115.2	119.2	0.79	165.4	±1.5
Z138	116.0	120.0	0.79	165.4	±1.5
Z139	116.8	120.8	0.79	165.4	±1.5
Z140	117.5	121.5	0.79	165.4	±1.5
Z141	118.2	122.2	0.79	165.4	±1.5
Z142	119.0	123.0	0.79	165.4	±1.5
Z143	119.8	123.8	0.79	165.4	±1.5
Z144	120.5	124.5	0.79	165.4	±1.5
Z145	121.2	125.2	0.79	165.4	±1.5
Z146	122.0	126.0	0.79	165.4	±1.5
Z147	122.8	126.8	0.79	165.4	±1.5
Z148	123.5	127.5	0.79	165.4	±1.5
Z149	124.2	128.2	0.79	165.4	±1.5
Z150	125.0	129.0	0.79	165.4	±1.5
Z151	125.8	129.8	0.79	165.4	±1.5
Z152	126.5	130.5	0.79	165.4	±1.5
Z153	127.2	131.2	0.79	165.4	±1.5
Z154	128.0	132.0	0.79	165.4	±1.5
Z155	128.8	132.8	0.79	165.4	±1.5
Z156	129.5	133.5	0.79	165.4	±1.5
Z157	130.2	134.2	0.79	165.4	±1.5
Z158	131.0	135.0	0.79	165.4	±1.5
Z159	131.8	135.8	0.79	165.4	±1.5
Z160	132.5	136.5	0.79	165.4	±1.5
Z161	133.2	137.2	0.79	165.4	±1.5
Z162	134.0	138.0	0.79	165.4	±1.5
Z163	134.8	138.8	0.79	165.4	±1.5
Z164	135.5	139.5	0.79	165.4	±1.5
Z165	136.2	140.2	0.79	165.4	±1.5
Z166	137.0	141.0	0.79	165.4	±1.5
Z167	137.8	141.8	0.79	165.4	±1.5
Z168	138.5	142.5	0.79	165.4	±1.5
Z169	139.2	143.2	0.79	165.4	±1.5
Z170	140.0	144.0	0.79	165.4	±1.5
Z171	140.8	144.8	0.79	165.4	±1.5
Z172	141.5	145.5	0.79	165.4	±1.5
Z173	142.2	146.2	0.79	165.4	±1.5
Z174	143.0	147.0	0.79	165.4	±1.5
Z175	143.8	147.8	0.79	165.4	±1.5
Z176	144.5	148.5	0.79	165.4	±1.5
Z177	145.2	149.2	0.79	165.4	±1.5
Z178	146.0	150.0	0.79	165.4	±1.5
Z179	146.8	150.8	0.79	165.4	±1.5
Z180	147.5	151.5	0.79	165.4	±1.5
Z181	148.2	152.2	0.79	165.4	±1.5
Z182	149.0	153.0	0.79	165.4	±1.5
Z183	149.8	153.8	0.79	165.4	±1.5
Z184	150.5	154.5			

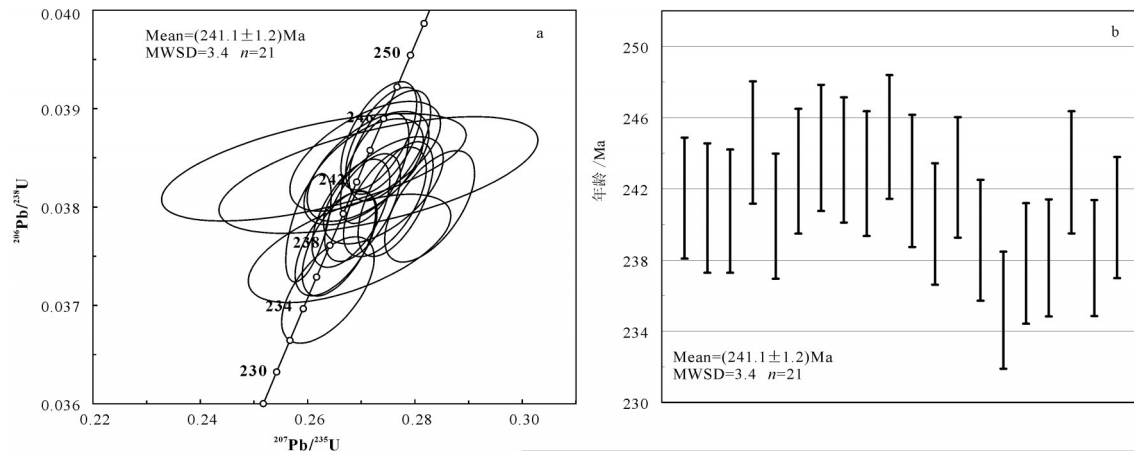


图4 阿拉思木辉长岩锆石U-Pb谐和年龄和加权平均年龄图
Fig.4 Zircon U-Pb concordia diagram and average age of Alasimu gabbro

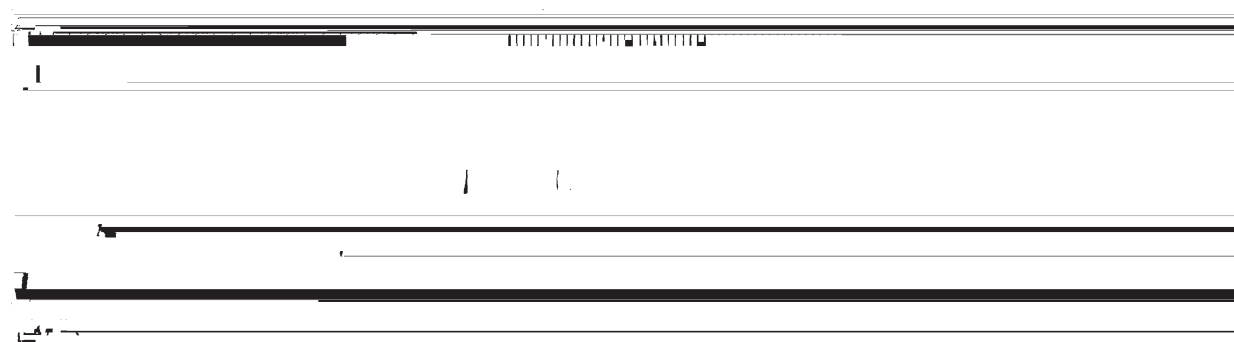


图5 阿拉思木辉长岩岩石分类图
Fig.5 Rock classification diagram of Alasimu gabbro

较高(10%~20%)时岩石部分熔融形成(邓晋福等, 2004)。

阿拉思木辉长岩富集大离子亲石元素, 亏损高场强元素, 具有弧岩浆岩特征, 显示该岩体为布青山—阿尼玛卿洋俯冲的结果(Sklyarow et al., 2003; Zhao et al., 2007), 且其样品具有较高的Nb/Ta比值(平均为15.4)和Zr/Hf比值(平均为36.5), 与洋中脊玄武岩值相近(Nb/Ta=17.7, Zr/Hf=36.19, 据Sun et al., 1989), 高于大陆地壳值(大陆地壳Nb/Ta=11, Zr/Hf=33, 据Sun et al., 1989), 指示镁铁质岩浆没有受到明显的地壳混染, 故可以基本排除地壳混染导致Nb/Ta亏损的特征。阿拉思木辉长岩较高的Ce/Th比值(9.08~18.76, 平均为12.53)、Ba/Th比值(155.92~268.17), 并且缺乏明显的Ce负异常($\delta\text{Ce}=1.32\sim1.61$, 平均为1.42), 表明受到俯冲洋壳沉积物的影响较弱, 这是由于俯冲洋壳沉积物熔体具有较高的Th(Pb)含量、低的Ce/Th(≈ 8)比值和Ba/Th(\approx

111)比值, 并呈现出明显的Ce负异常(Hole et al., 1984; Plank et al., 1998); 较低的Nb/U(2.96~7.98, 平均为5.38)、Ce/Pb(1.89~4.50, 平均为3.37)比值, 较高的Ba/Th比值(155.92~268.17, 平均为187.62)以及整体较高的Ba含量(平均为 61.14×10^{-6}), 暗示存在一定的流体作用(Seghedi et al., 2004); 图8a、8b也显示, 阿拉思木辉长岩受流体作用明显, 而受沉积物影响较弱, 同样图8c中投点均明显偏离MORB-OIB演化线, 也指示其形成受到俯冲组分的影响(Pearce et al., 1995), 与高铝玄武岩形成时富水环境相吻合。结合球粒陨石标准化REE配分曲线(图7a), 阿拉思木辉长岩显示出LREE的富集, 原始地幔标准化蛛网图中(图7b)明显富集LILE(Cs、Rb、Ba、K), 亏损HFSE(Nb、Ta、Ti、P), 也说明地幔源区受到了俯冲消减板片的影响, 为流体交代的富集地幔(Sajona et al., 2000; Hanyu et al., 2006; Tian et al., 2011)。

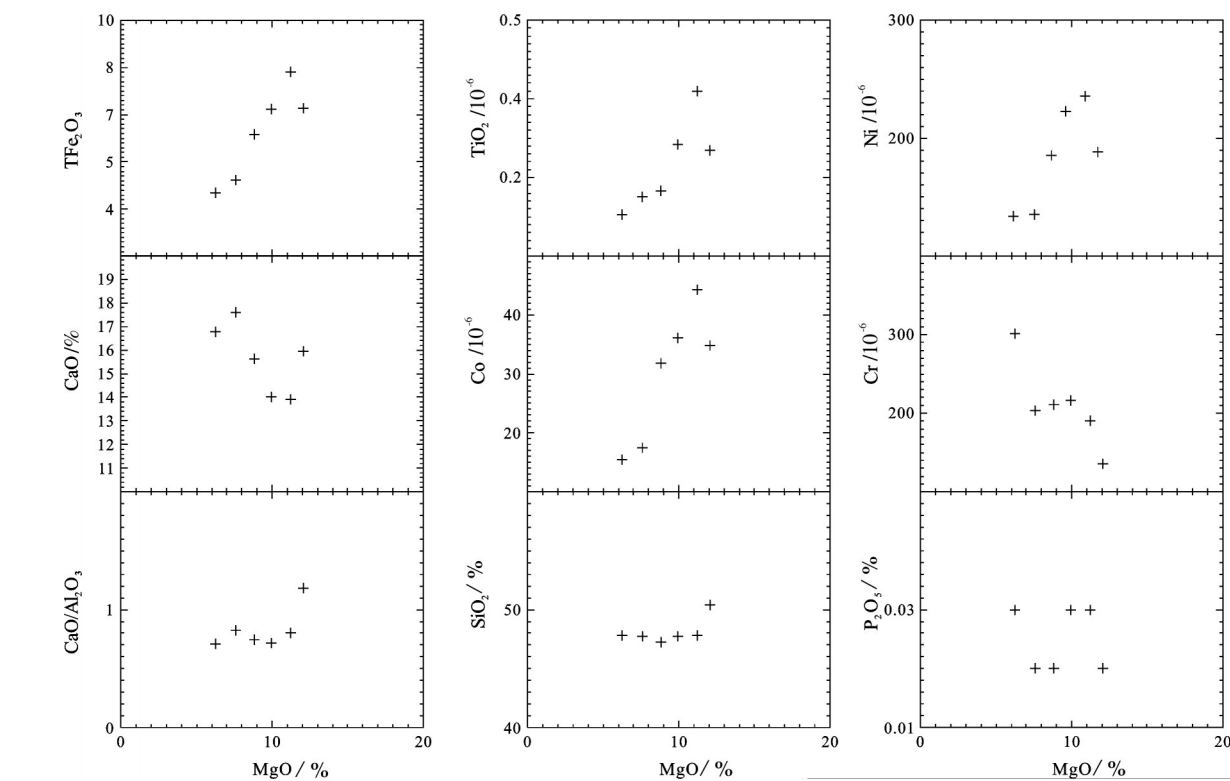


图6 阿拉思木辉长岩的Harker图解
Fig.6 The Harke diagrams of Alasimu gabbro

总之,阿拉思木辉长岩体源区为流体交代的富集地幔,源区相对富水,流体交代作用较强,岩浆演化过程中发生了弱的橄榄石和Ti-Fe氧化物的分离结晶,并且在上升过程中没有遭受明显的地壳混染。

5.2 构造环境

阿拉思木辉长岩的 TiO_2 含量较低(0.17%~0.37%,平均值为0.25%),明显低于MORB(1.5%)与OIB(>2.0%),相对接近岛弧岩浆岩(0.98%;(Pearce et al., 1982)), Al_2O_3 含量较高(13.1%~23.2%,平均值为18.9%),且具有明显消减带岩石的典型高铝特征(邓晋福等,2004)。微量元素也显示出岛弧玄武岩的特征,特别是Nb、Ta、Ti的负异常是岛弧岩浆岩的显著特征。微量元素Th/Ta比值为7.6~15.8,均大于3,显示为岛弧环境(Pearce et al., 1982);Nb/La比值0.17~0.45(<0.8),Hf/Ta比值(≥5),La/Ta比值(>15)Th/Nb比值(>0.07),进一步显示阿拉思木辉长岩具有岛弧玄武岩的特征(Condie,1989)。在La/Nb-La图解(李曙光等,1993)与Ti/1000-V图解(Pearce et al., 1973)中均落入岛弧玄武岩区域(图9)。由此表明阿拉思木辉长岩可能形成于岛弧环境。

5.3 构造意义

一般认为东昆仑南缘布青山—阿尼玛卿洋俯冲消减开始于晚二叠世(杨经绥等,2005;马昌前等,2015),伴随着洋壳向北俯冲,东昆仑地区出现与俯冲有关的岩浆岩和火山岩,例如具有岛弧岩浆岩特征的白日其利辉长岩体(熊富浩等,2011)、约格鲁辉长闪长岩(刘成东等,2004)、香加南山花岗岩基以及哈拉尕吐花岗岩基等(陈国超,2014),巴隆地区朝火鹿陶勒盖花岗闪长岩(陈功等,2016),这些岩体富集大离子亲石元素元素,亏损高场强元素,弧岩浆岩特征明显;发育在花石峡以东下大武至玛积雪山一带的火山岩,岩石总体上属于玄武岩-安山岩-流纹岩组合,其中以玄武安山质岩石为主,也形成于岛弧环境(杨经绥等,2005);此外,上二叠统格曲组底部角度不整合也是洋壳向北俯冲的沉积-构造响应(李瑞保等,2012)。在晚三叠世东昆仑地区进入到晚古生代—早中生代构造演化的后碰撞阶段,这些岩体主体具高钾钙碱性特征:例如小尖山辉长岩体(奥琮等,2015)、和勒冈希里可特花岗闪长岩体(陈国超等,2013)、科科额阿龙

表2 阿拉思木辉长岩主量(%)、微量元素(10^6)分析结果
Table 2 Major (%) and trace (10^6) elements analyses of Alasimu gabbro

样品号	XRD165-1	XRD165-2	XRD165-3	XRD165-4	XRD165-5	XRD165-6
岩性	辉长岩	辉长岩	辉长岩	辉长岩	辉长岩	辉长岩
SiO ₂	47.17	46.28	46.08	46.48	48.92	46.71
TiO ₂	0.20	0.21	0.28	0.37	0.27	0.17
Al ₂ O ₃	21.07	20.51	18.81	16.85	13.08	23.20
Fe ₂ O ₃ ^T	4.53	6.01	6.76	8.01	6.81	4.06
MnO	0.09	0.10	0.11	0.13	0.14	0.08
MgO	7.52	8.64	9.62	10.90	11.72	6.12
CaO	17.38	15.30	13.54	13.51	15.50	16.41
Na ₂ O	0.69	0.66	0.77	0.69	0.43	0.78
K ₂ O	0.10	0.17	0.56	0.25	0.20	0.18
P ₂ O ₅	0.02	0.02	0.03	0.03	0.02	0.03
LOI	0.79	2.60	2.47	1.34	1.55	1.25
TOTAL	99.56	100.50	99.03	98.56	98.64	98.99
FeO ^T	4.08	5.41	6.08	7.21	6.13	3.65
Mg [#]	76.69	74.02	73.82	72.95	77.32	74.92
Li	2.83	2.82	13.40	4.27	5.29	6.03
Be	0.18	0.16	0.34	0.20	0.08	0.16
Sc	35.10	27.69	25.53	31.06	45.67	22.86
V	132.52	116.00	112.71	155.09	178.86	98.22
Cr	202.76	211.33	216.48	190.84	135.60	301.37
Ni	135.43	185.70	222.25	235.28	188.42	134.12
Co	17.51	31.82	36.12	44.28	34.78	15.48
Cu	4.87	6.25	5.99	27.06	10.35	6.43
Zn	21.08	29.09	36.15	41.72	33.39	21.68
Ga	12.10	11.95	11.88	11.05	9.25	13.09
Rb	4.88	9.38	31.09	13.07	10.18	8.18
Sr	236.91	225.54	230.95	197.79	155.68	287.09
Y	3.93	3.68	4.94	5.07	5.27	3.47
Zr	6.86	9.62	20.94	16.30	10.86	7.22
Nb	0.24	0.46	0.99	0.93	0.42	0.34
Cd	0.07	0.10	0.07	0.10	0.11	0.06
In	0.02	0.02	0.02	0.03	0.03	0.02
Cs	1.26	1.57	3.79	1.86	1.64	0.81
Ba	34.77	44.37	113.10	65.03	40.77	68.77
La	1.00	1.36	2.64	2.07	1.23	1.94
Ce	2.43	3.10	5.67	4.72	3.18	4.08
Pr	0.36	0.42	0.73	0.63	0.49	0.52
Nd	2.22	2.44	3.94	3.59	3.02	2.78
Sm	0.70	0.68	1.01	0.99	0.97	0.76
Eu	0.24	0.23	0.28	0.27	0.25	0.27
Gd	0.66	0.62	0.83	0.86	0.86	0.63
Tb	0.11	0.11	0.14	0.14	0.15	0.11
Dy	0.71	0.67	0.89	0.92	0.97	0.65
Ho	0.14	0.14	0.18	0.19	0.21	0.13
Er	0.42	0.38	0.50	0.54	0.55	0.38
Tm	0.05	0.05	0.07	0.07	0.08	0.05
Yb	0.31	0.29	0.38	0.40	0.40	0.28
Lu	0.05	0.05	0.07	0.07	0.07	0.05
Hf	0.21	0.26	0.48	0.42	0.32	0.21
Ta	0.02	0.03	0.06	0.05	0.03	0.03
Pb	0.72	1.64	1.42	1.05	0.87	1.44
Bi	0.01	0.03	0.40	0.06	0.07	0.07
Th	0.13	0.22	0.62	0.39	0.26	0.44
U	0.05	0.07	0.18	0.12	0.12	0.11
δ Eu	0.88	0.81	0.65	0.65	0.69	0.87
δ Ce	1.32	1.32	1.41	1.45	1.41	1.61
Σ REE	9.39	10.54	17.32	15.46	12.43	12.63
(La/Yb) _N	2.18	3.17	4.68	3.49	2.07	4.68
(La/Sm) _N	0.90	1.26	1.64	1.32	0.80	1.61
(Gd/Yb) _N	1.71	1.73	1.76	1.74	1.74	1.83
(Tb/Yb) _N	1.58	1.61	1.65	1.60	1.66	1.66



图7 阿拉思木辉长岩球粒陨石标准化稀土元素配分曲线(a)和原始地幔标准化微量元素蛛网图(b)
(球粒陨石标准化数据据Boynton et al. ,1984; 原始地幔标准化数据据Sun et al. ,1989)

Fig.7 Chondrite-normalized REE patterns of Alasimu gabbro (a) and primitive mantle-normalized trace element patterns of Alasimu gabbro (b)
(chondrite-normalized data after Boynton et al., 1984; primitive mantle-normalized data after Sun et al., 1989)

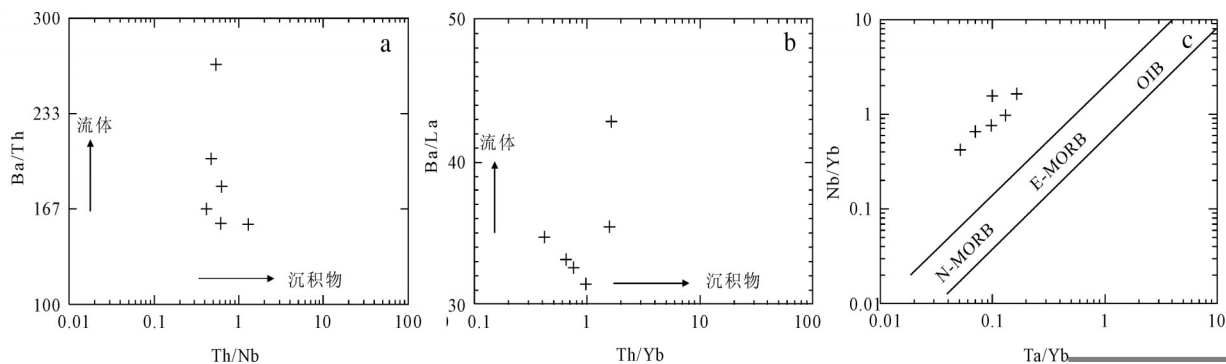


图8 阿拉思木辉长岩 Th/Nb–Ba/Th 图解(a, 据 Hanyu et al. , 2006)、Th/Yb–Ba/La 图解(b, 据 Woodhead et al. , 2001) 和 Th/Yb–Nb/Yb 图解(c, 据 Pearce et al. , 2008)

Fig.8 Th/Nb versus Ba/Th of Alasimu gabbro (a, after reference Plank et al., 1998), Th/Yb versus Ba/La of Alasimu gabbro (b, after Woodhead et al., 2001) and Th/Yb versus Nb/Yb of Alasimu gabbro (c, after Pearce et al. , 2008)

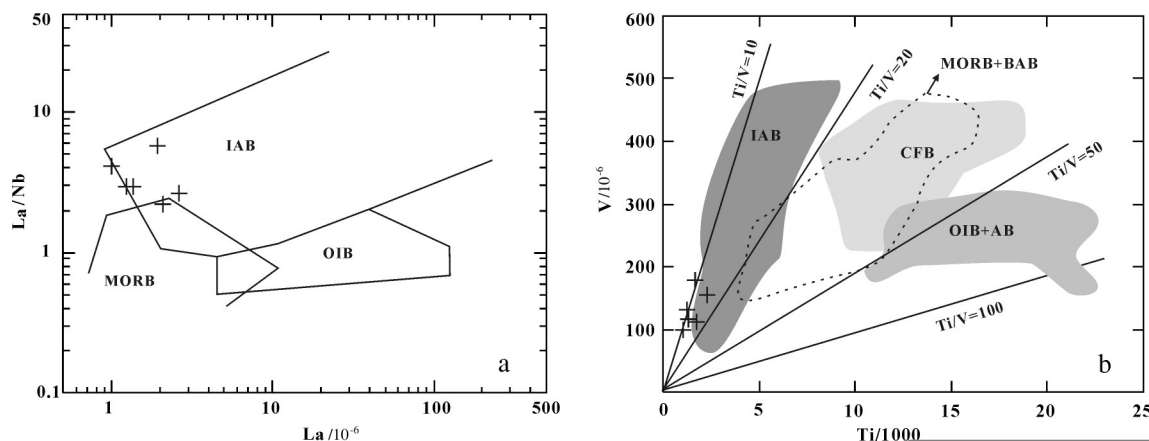


图9 阿拉思木辉长岩 La/Nb–La 图解(a, 据李曙光等, 1993) 和 Ti–V 图解(b, 据 Shervais. , 1982)
Fig.9 La/Nb–La of Alasimu gabbro (a, after Li Shuguang et al. , 1993), Ti/V of Alasimu gabbro (b, after Shervais. , 1982)

石英闪长岩体(陈国超,2014)、莫格通花岗闪长岩体(熊富浩,2014)等。然而对于东昆仑晚古生代—早中生代洋盆何时闭合、碰撞造山何时开始仍存在争议。莫宣学等(2007)通过对东昆仑造山带花岗岩及地壳生长研究认为239~242 Ma,华里西—印支旋回的俯冲结束/碰撞开始,但Huang et al.(2014)对东昆仑花岗岩研究认为,260~240 Ma布青山—阿尼玛卿洋已经闭合。Ding et al.(2014)对东昆仑花岗质岩脉研究认为,244 Ma的花岗质岩脉具有A2型花岗岩特征,暗示此时东昆仑进入到了后碰撞阶段。

阿拉思木辉长岩样品相对原始地幔富集大离子亲石元素(Rb、Ba、Sr等),明显亏损高场强元素(Nb、Ta、Ti等),显示为典型的岛弧环境产物,与东昆仑地区晚二叠世—早三叠世岛弧岩浆岩类似(莫宣学等,2007;刘成东等,2004;谌宏伟等,2005;李碧乐等,2012),明显不同于晚三叠世东昆仑地区与后碰撞伸展有关的镁铁质岩石(奥琮等,2015)。同时综合前文岩石成因及构造环境分析,认为阿拉思木镁铁质岩石是岛弧环境下受板片流体交代的岩石圈地幔部分熔融形成。然而,也有一些研究表明,在后碰撞伸展阶段形成的镁铁质岩石,由于继承古板片俯冲改造的地幔源区而往往具有类似于岛弧玄武岩的地球化学组成(EI et al.,2010;Wang et al.,2013)。阿拉思木辉长岩结晶年龄为中三叠世((241±1)Ma),明显早于东昆仑与陆陆碰撞有关的沉积—构造事件响应(李瑞保等,2012)(235 Ma,上三叠统八宝山组与中三叠统希里可特组和闹仓坚沟组之间的角度不整合),说明其不可能为碰撞后伸展的产物。本文报道的阿拉思木辉长岩体((241±1)Ma)可能代表了东昆仑晚古生代晚期—早中生代洋壳俯冲的最晚岩浆记录,并且代表了洋壳俯冲结束、碰撞开始的时限。而且,该辉长岩也明显不同于昆中蛇绿岩带内辉长岩。首先,形成时代不同,昆中蛇绿岩带内塔妥蛇绿岩、曲世昂蛇绿岩及清水泉蛇绿岩中辉长岩形成年龄介于481~522 Ma,且蛇绿岩中辉长岩与蛇绿岩套内蛇绿岩、辉橄榄岩、辉石岩组成蛇绿岩套(魏博,2015);昆中蛇绿岩带内阿次特蛇绿岩中玻安质辉长岩锆石U-Pb年龄为(510.0±5.2) Ma和(512.4±4.2) Ma(Li et al.,2017,待刊资料);此外,昆中蛇绿岩带均为东昆中构造带内,而巴隆地区阿拉思木辉长岩体位于东昆

北构造带。

此外,综合已有的区域地质资料可发现,260~240 Ma期间的岩浆岩明显具有岛弧岩浆岩的特征(莫宣学等,2007;杨经绥等,2005;马昌前等,2015;奥琮等,2015;刘成东等,2004;谌宏伟等,2005;李碧乐等,2012);238~230 Ma期间形成的岩浆岩以过铝质S型花岗岩为主,且分布较少(熊富浩等,2014;陈国超,2014),也暗示此阶段为陆陆主碰撞阶段;230~185 Ma期间以后碰撞伸展的岩浆岩为特征(陈国超等,2013;李佐臣等,2013;奥琮等,2015;熊富浩,2014;陈国超,2014)(图10),三个时期岩浆岩各具特点,并分别代表了洋壳俯冲阶段、同碰撞阶段以及后碰撞伸展阶段,同时李瑞保等(2012)对东昆仑地区若干不整合面的研究表明,上三叠统八宝山组与中三叠统闹仓坚沟组之间的微角度不整合也暗示中三叠世中期东昆仑地区古特提斯洋壳处于俯冲—碰撞转换阶段。进而可以认为东昆仑地区晚古生代晚期—早中生代洋盆最终关闭和碰撞造山作用的时代为中三叠世中期。

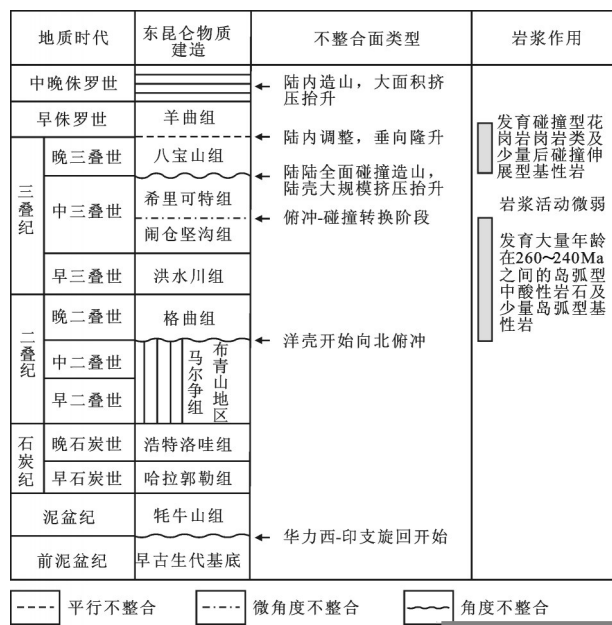


图10 东昆仑地区晚古生代—早中生代沉积—构造—岩浆演化简图(据李瑞保等,2012修改)

Fig.10 Late Paleozoic to Early Mesozoic sedimentary—magmatic evolution of East Kunlun area(after Li Ruibao et al., 2012)

6 结 论

(1)利用锆石U-Pb定年方法获得阿拉思木辉长岩体结晶年龄为(241±1)Ma,表明岩体形成时代为中三叠世中期。

(2)阿拉思木辉长岩体形成与板片流体交代的岩石圈地幔部分熔融有关,并且在形成过程中经历了弱的橄榄石和钛铁氧化物的分离结晶。

(3)阿拉思木辉长岩体可能代表了东昆仑造山带古特提斯洋壳俯冲的最晚岩浆记录,进而可以认为东昆仑造山带晚古生代—早中生代洋盆最终关闭和碰撞造山作用的时代为中三叠世中期。

致谢:衷心感谢审稿专家提出的宝贵修改意见和建议!

References

- Anderson T. 2002. Correction of common Pb in U-Pb analyses that do not report ^{204}Pb [J]. *Chemical Geology*, 192(1/2): 59–79.
- Ao Cong, Sun Fengyue, Li Bile, Wang Guan, Li Liang, Li Shijin, Zhao Junwei. 2015. U-Pb dating, geochemistry and tectonic implications of Xiaojianshan Gabbro in Qimantage Mountain, Eastern Kunlun Orogenic Belt[J]. *Geotectonica et Metaiogenia*, 39(6): 1176–1184 (in Chinese with English abstract).
- Bian Q T, Li D H, Pospelov, Yin L M, Li H S, Zhao D S, Chang C F, Luo X Q, Gao S L, AStrakhantsev Q and Chanov N. 2004. Age, geochemistry, and tectonic setting of Buqinshan ophiolite, North Qinghai-Tibet Plateau, China[J]. *Journal of Asian Earth Science*, 23(4): 577–596.
- Boynton W V. 1984. Geochemistry of the rare earth elements: meteorite studies[C]//Henderson P(ed.). *Rare Earth Element Geochemistry*, Elsevier, 63–114.
- Chen Guochao, Pei Xianzhi, Li Ruibao, Li Zuochen, Pei Lei, Liu Zhanqin, Chen Youxin, Liu Chengjun, Gao Jingmin, Wei Fanghui. 2013. Geochronology and genesis of the Helegang Xilikete granitic plutons from the southern margin of eastern East Kunlun Orogenic Belt and their tectonic significance[J]. *Chinese Journal of Geology*, 87(10): 1526–1541 (in Chinese with English abstract).
- Chen Guochao. 2014. Petrology, Genesis and Geological Significance of Late Paleozoic– Early Mesozoic Granitoids in East Kunlun Orogen[D]. Xi'an: Chang'an University, 1–182 (in Chinese with English abstract).
- Chen Hongwei, Luo Zhaohua, Mo Xuanxue, Liu Chengdong, Ke Shan. 2005. Underplating mechanism of Triassic granite of magma mixing origin in the East Kunlun orogenic belt[J]. *Geology in China*, 32(3): 386–395 (in Chinese with English abstract).
- Chen Youxin, Pei Xianzhi, Li Ruibao, Liu Zhanqing, Li Zuochen, Zhang Xiaofei, Chen Guochao, Liu Zhigang, Ding Sapeng, GuoJunfeng. 2011. Zircon U-Pb age of Xiaomiao Formation of Proterozoic in the eastern section of the East Kunlun Orogenic Belt[J]. *Geoscience*, 25(3): 510–521 (in Chinese with English abstract).
- Condie K C. 1989. Geochemical changes in basalts and andesites across the Archaean– Proterozoic boundary: Identification and significance [J]. *Lithos*, 23: 1–18.
- Deng Jinfu, Luo Zhaohua, Su Shangguo, Mo Xuanxue, Yu BingSun, Lai Xinyun, Chen Hongwei. 2004. Rock formation, tectonic environment and mineralization [M] Beijing: Geological Publishing House: 9–29 (in Chinese).
- Ding Q F, Jiang S Y, Sun F Y. 2014. Zircon U-Pb geochronology, geochemical and Sr-Nd-Hf isotopic compositions of the Triassic granite and diorite dikes from the Wulonggou mining area in the Eastern Kunlun Orogen, NW China: Petrogenesis and tectonic implications[J]. *Lithos*, 205: 266–283.
- Elaouli E H, Gasquet D, Cheilletz A. 2010. Lower Cryogenian calc-alkaline mafic rocks of the Western Anti-Atlas (Morocco): An example of orogenic-like magmatism in an extensional setting[J]. *Journal of African Earth Sciences*, 58(1): 81–88.
- Graham I J, Cole J W, Briggs R M, Gambled J A, Smith I E M. 1995. Petrology and petrogenesis of volcanic rocks from the Taupo Volcanic Zone: A review[J]. *Journal of Volcanology and Geothermal Research*, 68(1–3): 59–87.
- Hanyu T, Tatsumi Y, Nakai S, Chang Q, Miyazaki T, Sato K, Tani K, Shibata T, Yoshida T. 2006. Contribution of slab melting and slab dehydration to magmatism in the NE Japan arc for the last 25 Myr: Constraints from geochemistry[J]. *Geochemistry, Geophysics, Geosystems*, 7(8): doi: 10.1029/2005GC001220.
- Hole M J, Saunders A D, Marriner G F, Tamey J. 1984. Subduction of pelagic sediments: Implications for the origin of Ce-anomalous basalts from the Manana islands[J]. *Journal of the Geological Society, London*, 141(3): 453–472.
- Huang H, Niu Y L, Nowell G, Zhao Z D, Yu X H, Zhu D C, Mo X X and Ding S. 2014. Geochemical constraints on the petrogenesis of granitoids in the East Kunlun Orogenic belt, northern Tibetan Plateau: Implications for continental crust growth through syn-collisional felsic magmatism[J]. *Chemical Geology*, 370: 1–18.
- Li Bile, Sun fenyue, Yu Xiaofei, Qian Ye, Wang Guan, Yang Yinquin. 2012. U-Pb dating and geochemistry of diorite in the eastern section from eastern Kunlun middle uplifted basement and granitic belt[J]. *Acta Petrologica Sinica*, 28(4): 1163–1172 (in Chinese with English abstract).
- Li Huakun, Geng Jianzheng, Hao Shuang, Zhang Yongqin, Li Huimin. 2009. Study on the determination of zircon U-Pb isotopic age by laser ablation multireceiver plasma mass spectrometer (LA-MC-ICPMS)[J]. *Petrology and Geochemistry*, 28(Supp.): 600–601 (in Chinese).
- Li Ruibao, Pei Xianzhi, Li Zuochen, Liu Zhanqing, Chen Guochao, Chen Youxin, Wei Fanghui, Gao Jingmin, Liu Chengjun, Pei Lei. 2012. Geological characteristics of Late Palaeozoic– Mesozoic unconformities and their response to some significant tectonic events in eastern part of Eastern Kunlun[J]. *Earth Science Frontiers*, 19(5): 244–2547 (in Chinese with English abstract).
- Li Shuguang. 1993. Ba–Nb–Th–La diagrams used to identify tectonic

- environments of ophiolite [J]. *Acta Petrologica Sinica*, 9(2): 146–157 (in Chinese with English abstract).
- Li Zuochen, Pei Xianzhi, Li Ruibao, Pei Lei, Chen Guochao, Liu Chengjun, Chen Youxin, Gao Jingmin, Wei Fanghui, Wu Shukuan, Wang Yinchuan, Yang Jie. 2013. Geochronology and geochemistry of the Gerizhuotuo diorites from the Buqingshan tectonic Mélange belt in the southern margin of East Kunlun and their geologic implications[J]. *Chinese Journal of Geology*, 87(8): 1089–1103 (in Chinese with English abstract).
- Liu Chengdong, Mo Xuanxue, Luo Zhaohua, Yu Xuehui, Chen Hongwei, Li Shuwei, Zhao Xin. 2004. Mixing events between the crust- and mantle-derived magmas in Eastern Kunlun: Evidence from zircon SHRIMP chronology[J]. *Chinese Science Bulletin*, 49 (6): 592–602 (in Chinese with English abstract).
- Liu Zhanqing, Pei Xianzhi, Li Ruibao, Li Zuochen, Zhang Xiaofei, Liu Zhigang, Chen Guochao, Chen Youxin, Ding Sanping, Guo Junfeng. 2011. LA-ICP-MS zircon U-Pb geochronology of the two suites of ophiolites at the Buqingshan area of the Ányemáen Orogenic Belt in the southern margin of East Kunlun and its tectonic implication[J]. *Acta Geologica Sinica*, 85(2): 185–194 (in Chinese with English abstract).
- Ludwig K R. 2001. User's Manual for Isoplot/Ex.Version 2.49, A geochronological Tool- kit for Microsoft Excel[J]. Berkeley: Berkeley Geochronology Center Special Publication: 1–55.
- Ma Chanqian, Xiong F H, Yin S, Wang L X and Gao K. 2015. Intensity and cyclicity of orogenic magmatism: An example from a Paleo- Tethyan granitoid batholith, Eastern Kunlun, northern Qinghai- Tibetan Plateau[J]. *Acta Petrologica Sinica*, 31 (12) : 3555–3568 (in Chinese with English abstract).
- Maury R C, Fourcade S, Coulon C, El Azzouzi M, Bellon H, Coutelle A, Ouabadi A, Semroud B, Megartsi M, Cotton J, Belanteur O, Louni- Hacini A, Pique A, Capdevila R, Hernandez J, Rehault J. 2000. Post- collisional Neogene magmatism of the Mediterranean Maghreb margin: A consequence of slab breakoff[J]. *Earth and Planetary Science*, 331 (3): 159–137.
- Mo Xuanxue, Luo Zhaohua, Deng Jinfu, Yu Xuehui, Liu Chengdong, Chen Hong- wei, Yuan Wanming, Liu Yunhua. 2007. Granitoids and Crustal Growth in the East- Kunlun Orogenic Belt [J]. *Geological Journal of China Universities*, 13(3): 403– 414(in Chinese with English abstract).
- Morra V, Secchi F A G, Melluso L and Franciosi L. 1997. High-Mg subduction-related tertiary basalts in Sardinia, Italy[J]. *Lithos*, 40 (1): 69–91.
- Naumann T R and Geist D J. 1999. Generation of alkalic basalt by crystal fractionation of tholeiitic magma[J]. *Geology*, 27(5): 423– 426.
- Pearce J A and Peate D W. 1995. Tectonic implications of the composition of volcanic arc magmas[J]. *Annual Review of Earth and Planetary Sciences*, 23(1): 251–285.
- Pearce J A. 1982. Trace element characteristics of lavas from destructive plate boundaries [C]//Thorpe R S. Andesites: Orogenic Andesites and Related Rocks. Chichester: Willy: 525–548.
- Plank T, Langmuir C H. 1998. The chemical composition of subducting sediment and its consequences for the crust and mantle[J]. *Chemical Geology*, 145: 325–394.
- Sajona F G, Maury R C, Pubellier M, Leterrier J, Bellon H and Cotton J. 2000. Magmatic source enrichment by slab- derived melts in a young post- collision setting, central Mindanao (Philippines)[J]. *Lithos*, 54 (3/4): 173–206.
- Seghedi I, Downes H, Vaselli O, Szakacs A, Balogh K, Pecskay Z. 2004. Post- collisional Tertiary Quaternary mafic alkalic magmatism in the Carpathian- Pannonian region: A review[J]. *Tectonophysics*, 393: 43–62.
- Shervais J W. 1982. Ti-V Ti-V plots and the petrogenesis of modern and ophiolitic lavas[J]. *Earth and Planetary Science Letters*, 59 101 – 118
- Sklyarow E V, Gladkochub D P, Mazukabzov A M, Menshagin Yu V, Watanabe T, Pisarevsky S A. 2003. Neoproterozoic mafic dike swarms of the Sharyzhalgai metamorphic massif, southern Siberian craton[J]. *Precambrian Research*, 122(1): 359–376.
- Sun S S, McDonough W F. 1989. Chemical and isotopic systematics of oceanic basalts: Implications for mantle composition and processes[C]//Saunders A D, Norry M J. *Magmatism in the Ocean Basins*. Geological Society, London, Special Publication, 42: 313– 345.
- Takazawa E, Frey F A, Shimizu N, Obata M, Bodinier J L. 1992. Geochemical evidence for melt migration and reaction in the upper mantle[J]. *Nature*, 359(3906): 55–58.
- Tatsumi Y and Ishizaka K. 1981. Existence of andesitic primary magma: an example from southwest Japan[J]. *Earth and Planetary Science Letters*, 53: 124–130.
- Taylor S R, McLennan S M. 1985. *The Continental Crust: Its Composition and evolution*[M]. Oxford: Blackwell Scientific Publication: 1–132.
- Tian L Y, Castillo P R, Hilton D R, Hawkins J W, Hanan B B, Pietruszka A J. 2011. Major and trace element and Sr-Nd isotope signatures of the northern Lau Basin lavas: Implications for the composition and dynamics of the back- arc basin mantle [J]. *Journal of Geophysical Research*, 116: doi: 10.1029/2011JB008791.
- Wang Guocan, Wei Qinrong, Jia Chunxin, Zhang Kexin, Li Deweii, Zhu Yunhai, Xiang Shukuan. 2007. Some ideas of Precambrian geology in the East Kunlun, China[J]. *Geological Bulletin of China*, 26(8) : 929– 937(in Chinese with English abstract).
- Wang Y J, Zhang A M, Fan W M, Zhang Y H, Zhang Y Z. 2013. Origin of paleosubduction modified mantle for Silurian gabbro in the Cathaysia Block: Geochronological and geochemical evidence[J]. *Lithos*, 160–161: 37–54.
- Wei Bo. 2015. Study on the Geological Characteristic and Tectonic Attribute of the Ophiolite and Tectonic Attribute of the Ophiolite and Island-arc-type Ingenous Rocks, Central Belt of East Kunlun (Esatern Sectiong) [D]. Xi'an: Chang'an University, 1– 132(in Chinese with English abstract).
- Wilson M. 1989. *Igneous Petrogenesis: A Global Tectonic Approach*[M]. London: Unwin Hyman, 1–466.
- Woodhead J D, Hergt J M, Davidson J P and Eggins S M. 2001. Hafnium isotope evidence for ‘conservative’ element mobility

- during subduction zone processes[J]. Earth and Planetary Science Letters, 192(3): 331–346.
- Xiong Fuhao, Ma Chanqian, Zhang Jinyang, Liu Bin, Jiang Hongan, Huang Jian. 2011. Zircon LA-ICP-MS U-Pb dating of Bairiqili gabbro pluton in East Kunlun orogenic belt and its geological significance[J]. Geological Bulletin of China, 30(8): 1196–12027 (in Chinese with English abstract).
- Xiong Fuhao. 2014. Spatial-temporal Pattern, Petrogenesis and Geological Implication of Paleo-Tethyan Granitoids in the East Kunlun Orogenic Belt(Eastern Segment) (D). Wu Han: China University of Geoscience(Wu Han), 1–174 (in Chinese with English abstract).
- Xu Zhiqin, Yang Jinshui, Li Haibing, Yao Jianxin. 2006. The Early Palaeozoic terrane framework and the formation of the high-pressure(HP) and ultra-high pressure(UHP) metamorphic belts at the Central Orogenic Belt(COB)[J]. Acta Geologica Sinica, 80(12): 1793–1806 (in Chinese with English abstract).
- Yan Jingsui, Xu Zhiqin, Li Haibing, Shi Rendeng. 2005. The paleo-Tethyan volcanism and plate tectonic regime in the A'nyemaqen region of East Kunlun, northern Tibet Plateau[J]. Acta Petrologica et Mineralogica, 24(5): 369–380 (in Chinese with English abstract).
- Yang Jingsui, Xu Zhiqin, Ma Changqian, WuCailai, Zhang Jianxin, Wang Zhongqi, Wang Guocan, Zhang Hongfei, Dong Yunpeng, Lai Shaocong. 2010. Compound orogeny and scientific problems concerning the Central Orogenic Belt of China[J]. Geology in China, 37(1): 1–11 (in Chinese with English abstract).
- Yin Hongfu, Zhang Kexin, Chen Nengsun, Wang guocan, Hou guangjiu, Zhu Yunhai, Bai Yunshan, Zhang Zhi, Wang Yunbiao, Li Changan. 2003. The People's Republic of China Regional Geological Report: 1: 250000 Donggi Conag Hu Map[R]. Wuhan: China University of Geosciences Press, 60–80 (in Chinese with English abstract).
- Zhao J H and Zhou M F. 2007. Geochemistry of Neoproterozoic mafic intrusions in the Panzihua district (Sichuan Province, SW China): Implications for subduction-related metasomatism in the upper mantle[J]. Precambrian Research, 152(1/2): 27–47.

附中文参考文献:

- 奥琮, 孙丰月, 李碧乐, 王冠, 李良, 李世金, 赵俊伟. 2015. 东昆仑祁漫塔格地区小尖山辉长岩地球化学特征、U-Pb年代学及其构造意义[J]. 大地构造与成矿学, 39(6): 1176–1184.
- 陈国超, 裴先治, 李瑞保, 李佐臣, 裴磊, 刘战庆, 陈有忻, 刘成军, 高景明, 魏方辉. 2013. 东昆仑造山带东段南缘和勒冈希里可特花岗岩体时代、成因及构造意义[J]. 地质学报, 87(10): 1526–1541.
- 陈国超. 2014. 东昆仑造山带(东段)晚古生代—早中生代花岗岩质岩石特征、成因及地质意义[D]. 西安: 长安大学, 1–182.
- 陈有忻, 裴先治, 李瑞保, 刘战庆, 李佐臣, 张晓飞, 陈国超, 刘智刚, 丁仁平, 郭俊锋. 2011. 东昆仑造山带东段元古界小庙岩组的锆石U-Pb年龄[J]. 现代地质, 25(3): 510–521.
- 谌宏伟, 罗照华, 莫宣学, 刘成东, 柯珊. 2005. 东昆仑造山带三叠纪岩浆混合成因花岗岩的岩浆底侵作用机制[J]. 中国地质, 32(3): 386–395.
- 邓晋福, 罗照华, 苏尚国, 莫宣学, 于炳孙, 赖兴运, 谌宏伟. 2004. 岩石成因、构造环境与成矿作用[M]. 北京: 地质出版社, 9–29.
- 李碧乐, 孙丰月, 于晓飞, 钱烨, 王冠, 杨廷琨. 2012. 东昆仑东段闪长岩U-Pb年代学和岩石地球化学研究[J]. 岩石学报, 28(4): 1163–1172.
- 李怀坤, 耿建珍, 郝爽, 张永清, 李惠民. 2009. 用激光烧蚀多接收器等离子体质谱仪(LA-MC-ICP-MS)测定锆石U-Pb同位素年龄的研究[J]. 矿物岩石地球化学通报, 28(增刊): 600–601.
- 李瑞保, 裴先治, 李佐臣, 刘战庆, 陈国超, 陈有忻, 魏方辉, 高景明, 刘成军, 裴磊. 2012. 东昆仑东段晚古生代—中生代若干不整合面特征及其对重大构造事件的响应[J]. 地学前缘, 19(5): 244–254.
- 李曙光. 1993. 蛇绿岩生成构造环境的Ba-Th-Nb-La判别图[J]. 岩石学报, 9(2): 146–157.
- 李佐臣, 裴先治, 刘战庆, 李瑞保, 裴磊, 陈国超, 刘成军, 陈有忻, 高景民, 魏方辉, 吴树宽, 王银川, 杨杰. 2013. 东昆仑南缘布青山构造混杂岩带哥日卓托闪长岩年代学、地球化学特征及其地质意义[J]. 地质学报, 87(8): 1089–1103.
- 刘成东, 莫宣学, 罗照华, 喻学惠, 谌宏伟, 李述为, 赵欣. 2004. 东昆仑壳-幔岩浆混合作用: 来自锆石SHRIMP年代学的证据[J]. 科学通报, 49(6): 592–602.
- 刘战庆, 裴先治, 李佐臣, 张晓飞, 刘智刚, 陈国超, 陈有忻, 丁仁平, 郭俊锋. 2011. 东昆仑南缘阿尼玛卿构造带布青山地区两期蛇绿岩的LA-ICP-MS锆石U-Pb定年及其构造意义[J]. 地质学报, 85(2): 185–194.
- 马昌前, 熊富浩, 尹炼, 王连训, 高珂. 2015. 造山带岩浆作用的强度和旋回性: 以东昆仑古特提斯花岗岩类岩基为例[J]. 岩石学报, 31(12): 3555–3568.
- 莫宣学, 罗照华, 邓晋福, 喻学惠, 刘成东, 谌宏伟, 袁万明, 刘云华. 2007. 东昆仑造山带花岗岩及地壳生长[J]. 高校地质学报, 13(3): 403–414.
- 王国灿, 魏启荣, 贾春兴, 张克信, 李德威, 朱云海, 向树元. 2007. 关于东昆仑地区前寒武纪地质的几点认识[J]. 地质通报, 26(8): 929–937.
- 魏博. 2015. 东昆仑中构造带(东段)蛇绿岩与岛弧型侵入岩地质特征及构造属性研究[D]. 西安: 长安大学, 1–132.
- 熊富浩, 马昌前, 张金阳, 刘彬, 蒋红安, 黄坚. 2011. 东昆仑造山带白日其利辉长岩体LA-ICP-MS锆石U-Pb年龄及地质意义[J]. 地质通报, 30(8): 1196–1202.
- 熊富浩. 2014. 东昆仑造山带东段古特提斯域花岗岩类时空分布、岩石成因及其地质意义[D]. 武汉: 中国地质大学(武汉), 1–174.
- 许志琴, 杨经绥, 李海兵, 姚建新. 2006. 中央造山带早古生代地体构架与高压/超高压变质带的形成[J]. 地质学报, 80(12): 1793–1806.
- 杨经绥, 许志琴, 李海兵, 史仁灯. 2005. 东昆仑阿尼玛卿地区古特提斯火山作用和板块构造体系[J]. 岩石矿物学杂志, 24(5): 369–380.
- 杨经绥, 许志琴, 马昌前, 吴才来, 张建新, 王宗起, 王国灿, 张宏飞, 董云鹏, 赖绍聰. 2010. 复合造山作用和中国中央造山带的科学问题[J]. 中国地质, 37(1): 1–11.
- 殷鸿福, 张克信, 陈能松, 王国灿, 候光久, 朱云海, 拜永山, 张志, 王永标, 李长安. 2003. 中华人民共和国区域地质调查报告: 1: 250000 冬给措纳湖幅[R]. 武汉: 中国地质大学出版社, 60–80.